Magnetism and Superconductivity in Hydrogenated Graphite Foils

Nadina Gheorghiu

UES Inc., Dayton, OH 45432

Charles R. Ebbing

University of Dayton Research Institute, Dayton, OH 45469

Timothy J. Haugan

The Air Force Research Laboratory (AFRL), Aerospace Systems Directorate, AFRL/RQ, Wright-Patterson AFB, OH 45433

Abstract

Unique to certain unconventional superconductors is the coexistence of magnetism and superconductivity. We have recently found ferromagnetism and superconductivity in hydrogenated graphitic materials (1). Herein we present similar findings for hydrogenated graphite foils. As the strength of the magnetic field is increased, the temperature-dependent magnetization shows several important transitions: from a Néel paramagnetic-antiferromagnetic transition, to a ferromagnetic superconductor state, to an orbital paramagnetic glass high-temperature superconductor with critical temperature $T_c \sim 50-60$ K. Thus, the magnetism of hydrogenated low-density carbon graphite foils plays an important role in establishing high-temperature electronic correlations. The ferromagnetic superconducting state is observed up to room temperature, proving that spin-orbit coupling and strong electron-electron correlations are both leading to high-temperature superconductivity in these materials.

Keywords: high-temperature ferromagnetic superconductor, Little model for an organic superconductor, orbital paramagnetic glass

Email address: Nadina.Gheorghiu@yahoo.com (Nadina Gheorghiu)

1. Introduction

Until relatively recently, magnetism and superconductivity (SC) where thought as mutually exclusive states of matter. In cuprates, high-temperature superconductivity (HTSC) emerges from tuning the charge-doping of the parent phase, an antiferromagnetic (AFM) Mott insulator. The emergence of new SC materials like the (iron-based) pnictides clarified the important role played by long-range magnetic spin correlations in the coexistence of magnetism and SC on the mesoscopic scale. A ferromagnetic domain (FM) can transfer the magnetically stable spin-triplets into the neighboring nonmagnetic domains and the latter becomes SC. Furthermore, long-range proximity effects are established at the SC/FM interfaces. In addition, anisotropic materials might contain magnetically soft/hard or FM/AFM domains that are interfacially coupled, leading to the formation of quasi-Bloch walls. Under an applied reversed field, the quasi-Bloch walls are moving from within the FM domains to being compressed against the hard AFM domains. The magnetization is reversible and anisotropic (2).

In this paper, we are bringing forth new research on magnetic and SC transitions in hydrogenated graphite foils. This is a continuation as well as a reinforcement of our previous research on magnetic and SC properties of hydrogenated graphitic fibers (1; 3). The carbon (C) allotrope in this case is the graphite foil, i.e., exfoliated graphite. In pregraphitic materials such as exfoliated graphite or C fibers, the graphite layers are randomly stacked forming a turbostratic structure. This is in contrast to the regular stacking found in graphite crystals, where the ideal structure consists of C atoms arranged in a hexagonal/honeycomb pattern with the parallel graphene layers at $\bar{c} = 3.35$ Å distance apart (the out-of-plane lattice constant) weakly interacting by Van der Waals forces. In-plane, each C atom is covalently bonded to three other C atoms at the distance $\bar{a} = 1.42$ Å (the in-plane lattice constant) through sp^2 sp^2 axial hybrid orbital overlap. This layered structure of graphite leads to highly anisotropic physical properties. Ion-implantation, heat treatment, hydrogenation, or oxidation result in sp^2 to sp^3 bond conversion. Distorted sp^2 C bonds form grain boundaries. Importantly, disorder in the stacking sequence leads to two-dimensional (2D) weak-localization of electrons thereby to electron-electron ($e - e$) interactions with some potentially turning into SC correlations. While the σ electrons are localized, the π electrons are free to move just as conduction electrons in metals and their long-range correlations result in FM. The addition of non-magnetic (orbital)

atoms like hydrogen (H) results in FM. Hydrogenated graphene was predicted for being FM (4) and this is what we have indeed found [Gheorghiu1]. Intrinsically, graphite is already magnetic: there are AFM correlations between unlike sublattices (ABAB...) and FM correlations between like sublattices (AAA... or BBB...). In addition, disorder-induced magnetism and 2D weak-localization of electrons can lead to SC correlations as we have uncovered for oxygen-implanted C-based materials (5; 6) as well as for boron-doped C-based materials (7).There, we have found for the dominant SC fraction that the critical temperature is in the range $T_c \sim 50 - 80$ K. Our findings agree with an earlier estimate that the shielding fraction, hence T_c, of metal-doped aromatic hydrocarbons increases with an increasing number of benzene rings (8). The results presented here are in agreement with our previous work, thus confirming that hydrogenated graphite is a HTSC.

2. Experiment

The materials used in this work are graphite foil (Graphtek) square samples with dimensions 2 mm × 2 mm × 1 mm. The hydrogenation was done via doping by a hydrocarbon (octane, C_8H_{18}), resulting in what we will refer as H-C foils. The four-wire Van Der Pauw square-pattern technique was used for electrical measurements. The quality of the silver electrical contacts was checked using an Olympus BX51 microscope. Magneto-transport and magnetization measurements were carried out in the 1.9 K - 300 K temperature (T) range and for magnetic fields of induction B up to 9 T using the Quantum Design Physical Properties Measurement System (PPMS) model 6500. The transport data was acquired using a direct current $I = 20$ μA.

3. Results and Discussion

Resistivity measurements for a H-C foil sample are shown in Fig. 1, with data plotted relative to the value at $T = 300$ K. The hydrogenation decreases the C foils resistivity by one order of magnitude, $\rho_{H-C}(T = 300$ K,$B = 0) \simeq 72$ $\mu\Omega\cdot$ cm vs. $\rho_C(T = 300$ K,$B = 0) \simeq 800$ $\mu\Omega\cdot$cm for the raw C foil. When a magnetic field is applied perpendicularly to the sample's area, we find: a) asymmetry in the resistance data for B_+ vs.the B_- values caused by the effect of the thermal gradient and Lorenz force on electrons vs. holes leading to charge imbalance, nonlocal resistance (9), or possible excitonic SC; b) higher/lower R for increasing values of $|B|$; c) convergence

of all $R(T, B)$ values for $T \sim 250 - 280$ K, a temperature range that was found relevant in our previous work (1; 3; 5; 6). Notice that in the case of the excitonic SC found in the H-C-N fibers (1), the Lorentz force is the same on an electron as on a hole. Thus, there is no imbalance between the number of electrons and the number of holes. I.e., the AFM and SC states can coexist (1).

It is important to notice that the coefficient of thermal expansion along the c-axis (normal to the graphitic planes) is negative and in absolute value larger than the in-plane coefficient of thermal expansion, both of the order of 10^{-6}/K. In C fibers and in graphite, the former is about $3\times$ larger, while in graphite foil it is about $50\times$ larger. Thus, heating of the sample results in a decrease of the inter-layer distance. The effect is similar to what one would expect from applying pressure to the layered graphitic system in the direction of the c-axis. In addition, a transverse magnetic field results in a corresponding pressure applied on the 2D material, enhancing the anisotropy in the electronic transport. At the maximum field induction here, $B = 9$ T, the corresponding magnetic pressure is $p_{mag} \simeq 32$ GPa. Without staggering and with a lower inter-layer distance, the graphite foil (or graphite, for that matter) would be SC just as MgB_2 is. The electronic similarities between graphite and other systems like MgB_2 or Bi_2Se_3 are described within the resonating-valence-bond model (10).

We have also conducted magnetization measurements using the PPMS vibrating sample magnetometry option. The temperature-dependent magnetization data is shown in Fig. 2. Will be there a Meissner effect, arguably the most essential property of a SC that also implies zero resistivity? At the cooling of a SC placed in a magnetic field, the initially trapped magnetic flux should be expelled below the SC transition temperature T_c. As Fig. 2 shows, upon incrementally increasing the strength of the magnetic field H from 0 to 150 Oe, several important magnetic transitions occur in the H-C foil: from reversible to irreversible paramagnetism (PM) (Fig. 2a-c), to slightly irreversible PM-AFM Néel transition (Fig. 2d-f), to reversible diamagnetism (DM) (Fig. 2g), and further more to irreversible DM (Fig. 2h-i). We find for the Néel transition temperature $T_N \simeq 44$ K (Fig. 2d-f). Significantly, when the strength of the magnetic field is high enough, the Meissner fraction becomes dominant and the H-C foil becomes SC below $T_c \simeq 57$ K (Fig. 2h-i). In addition, we observe low-T upturn of the zero-field cooled (ZFC) and the field-cooled (FC) curves. This reentrant PM was observed in other high-T_c systems (11) and attributed to the magnetization of the SC coming from

three sources: (a) the DM shielding moment; (b) trapped flux; (c) a PM contribution (positive magnetic susceptibility χ_m). The Meissner fraction depends strongly on the strength of the applied field. In the high-field limit, the trapped flux fraction can be comparable to and eventually can cancel out the DM shielding fraction. This kind of Meissner effect is PM by nature due to the trapping of magnetic flux (12). On decreasing T, the magnetic flux captured at the third (surface) critical field inside the SC sheath compresses into a smaller volume, thus allowing extra flux to penetrate at the surface (13). The PM Meissner effect is a general property of a small SC that being enhanced in a plate geometry, such as our graphite foil here. Moreover, in granular SC (which are type II SC), the occurrence of the PM Meissner effect proves the existence of π Josephson-coupled SC domains. The PM Meissner effect was also observed in FM-SC heterostructures (14). The PM is actually metastable. At a second run under the same magnetic field strength, the magnetization is negative, and a cusp left from the Néel point can still be seen, though at a higher value, $T \simeq 49$ K (Fig. 2f). The change in magnetization sign from positive to negative shows that the trapped magnetic flux was removed from the system, which is now being driven into the SC state, apparently a more stable state than the PM one. After all, the graphite foil has irregular zig-zag edges and thus it can host PM, FM, AFM, DM, and even SC. As we will see later on, the only way to accommodate AFM, PM, and SC is to have a FM that is also a SC, i.e., a triplet-spin ferromagnetic superconductor (FMSC).

Upon further increase in the strength of the magnetic field H, the magnetization becomes again positive and the PM-AFM Néel transition reemerges at the same transition temperature $T_N \simeq 44$ K (Fig. 3). It is as if in higher magnetic fields, a reentrant PM order emerges by overcoming the SC order. As Fig. 4 shows, the system is not a glass, or the irreversible temperature T_{irrev} would need to vary linearly with $H^{2/3}$ accordingly to the Almeida-Thouless scaling law. The behavior at magnetic field strength $H \sim 150$ Oe (upper line above $T_c \simeq 57$ K) is similar to the $H - T_c$ line in (11) for a granular SC. The reentrance of PM and of the PM-AFM Néel transition can be explained by considering that the H-C foil is an example of orbital PM glass HTSC, a true new state of matter in which one can find the coexistence of orbital PM order and SC order without the Meissner effect (15). The orbital glass is like a crystal with chaotically distributed dislocations of different types such that even a small magnetic field can polarize the system by inducing different orbital moment-flip processes. The strength of the

5

chaotically distributed circular currents can decrease and increase in time or even change direction (i.e., have orbital moment flips). The rate of change for these currents will depend on the local dissipation in the weak links that is due to impurities and the local H, which in turn will depend on the values of other orbital currents. The SC regions form thick rings of Josephson junctions and the magnetic flux going through the interior of the SC rings is a chaotic line (linear, circular, other), i.e., it is a topological object. Thus, the system is an orbital glass and a SC at the same time, moreover, it can be a HTSC. In addition, granular disordered HTSC might have the sign of some of their Josephson loops reversed when π-contacts are being created between SC grains by the presence of magnetic impurities. In the H-C foil here, itinerant FM is introduced in the system by octane with its freely moving H^+ (protons) on the graphite s interfaces. Thus, the Josephson junction SC (JJSC) loops might have π-contacts. The formation of the PM orbital glass is conditioned as follows: a) the JJSC rings with an even number of π-contacts give constant negative magnetic susceptibility , i.e. conventional Meissner response, while b) the JJSC rings with an odd number of π-contacts give (positive) PM susceptibility, which is proportional to $1/H$. Clearly, $\chi_m \to 0$ as $H \to 0$ (abnormal response). At any number of JJSC rings there will exist a small H for which the rings will give the main contribution to χ_m, which will be PM. The systems behavior is of a magnet with local orbital magnetic moment. On the other hand, the magnitude of the anti-Meissner signal decreases with increasing H and, for sufficiently large H, $\chi_m < 0$, i.e., the DM Meissner effect. As Figs. 2-3 show, SC dominates over PM for 100 Oe $< H < 200$ Oe. The rather small magnetization observed for $H \sim 175 - 200$ Oe (Fig. 3c) suggests possible clustering of superparamagnetic (SPM) order for field strengths smaller than needed for the reentrant PM that eventually will coexists with a SC order for $H \sim 300$ Oe. An intermediate SPM order can be seen as transitory form of magnetism proceeding the reentrance of orbital PM glass coexisting with SC. A persistent AFM/FM background for temperatures up to 50-60 K (1), which coming from the free H^+ protons, might favor the occurrence of different magnetic orders, as well as the orbital glass behavior. For comparison, the ZFC-FC data for a raw foil (C-foil), O-implanted (O-foil), and a C foil hydrogenated by octane treatment (H-C foil) are shown in Fig. 5. The critical temperatures T_c are 55 K, 50 K, and 57 K, respectively. These values are all close to the mean-field T_c for SC correlations in metallic-H multilayer graphene or in HOPG, $T_c \sim 60$ K (16). Interestingly, the remanent magnetization for the raw C foil clearly

shows that the critical temperature $T_c \simeq 55$ K separates the low-T PM orbital glass (Fig. 5, upper lot) from the high-T FM background FM (Fig. 5, lower plot). Note that SPM, which we have found before (7), can lead to large magnetocaloric effect and giant or even colossal magnetoresistance (5), which have significant technological applications to magnetic refrigeration or to the use of spin-injection for achieving dissipationless (using triplet FMSC) long-distance transport and reading/writing of information in the new field of spintronics. Thus, one can infer that SPM is one of the dynamic features of C-based materials. Likely, the PM-SPM-PM transitions occur while magnetic domains change their volumes as the strength of the magnetic field is increased.

For moderate field strengths $H \geq 200$ Oe, the PM dominates. We observe both reentrant PM and more PM-AFM Néel transitions in the H-C foil, the latter occurring at the same $T_N \simeq 44$ K (Fig. 3d-f). To our knowledge, these are completely new features, for which a new mechanism would be needed to explain both the coexistence of SC and orbital glass PM as well as the reentrant features observed in the H-C system. In high magnetic fields, the SC and the PM orbital glass are decoupled when the field direction is reversed and either DM ($\chi_m < 0$) or PM ($\chi_m > 0$) wins (Fig. 1).

High-field magnetization loops $m(B)$ at temperatures $T = 2.5$ K and $T = 300$ K are shown in Fig. 6. In order to separate the SC/FM response from the huge DM background, the sample' s DM response to a high field ($B = 1$ T, inset) was subtracted from the initial data (inset). Several important features we observe with these $m(B)$ loops: a) they have both FM and DM trends for all temperatures below 300 K, suggesting that the Curie temperature for these H-C foils is higher than the room temperature; b) after the subtraction of the DM background, they have an oscillatory dependence on the field, confirming the existence of the PM Meissner effect in these H-C foils and surface SC manifested as a metastability that is due to the coexistence of multi-quanta vortex states ($L\Phi_0, \Phi_0 = h/2e, L > 1$) and single quantum ($L = 1$, or Abrikosov) vortices (17); c) as T goes up, the FM component increases at the expense of the PM component.

Low-field $m(B)$ loops are shown in Fig. 7. Here too we notice several important features: a) at low T, the loops are not hysteretic, a characteristic of soft materials such as graphite foil; b) both the FM and the SC, or the FMSC, are pronounced in the H-C foil as compared to the C foil; c) the $m(B)$ the loops show the kink feature characteristic to granular SC; d) the hysteresis increases with the temperature and the FMSC becomes more evident beyond

7

the low-T PM.

A couple of low-field $m(B)$ loops are zoomed in in Fig. 8. For the inner loop, the critical values for the magnetic induction of this type II SC is of the order of few tens of mT, $B_{c1} \simeq 10$ mT and $B_{c2} \simeq 30$ mT. We use these values to estimate the penetration depth $\lambda \sim 250$ nm and the coherence length $\xi \sim 100$ nm, respectively. The ratio $\kappa = \lambda/\xi \simeq 2.5 > 0.42$ tells us that there is a SC surface layer for which a third maximum field B_{c3} can be defined (18) such that $B_{c3} = 2.4\kappa B_{c1} = 1.7B_{c2}$. Here, we find then $B_{c3} \simeq 51 - 60$ mT. It should be pointed out that for ideal samples, the nucleation of SC regions is energetically favored to start from the samples' surface. In non-ideal samples like the ones here, the nucleation of SC regions in decreasing field is rather initiated from volume defects. It is possible that a bulk SC state (hugely-gaped) is found at $T_c \simeq 50 - 60$ K, while surface (topological) SC states (weakly-gaped), which are protected by the time-reversal symmetry, are found at all other temperatures. The hugely gaped (bulk) excitonic state at and the T-dependence of the SC gap found in (1) showed that the hydrogenated graphitic system can host both bulk (characteristic to Bernal stacking) and flat-band surface states (characteristic to rhombohedral stacking).

We should also mention that, in order to observe the unaltered effects of octane on the C foil, the $m(B)$ loops were taken without prior flux cleaning (i.e.,degaussing). Nevertheless, a degaussing of the sample is shown in Fig. 9.

The hydrogenation of the C foil done by intercalation with octane showed an interesting time behavior. As the C foil was kept in octane for a longer period of time, the FM fraction increased as a result of longer time exposure to etching (Fig. 10). It is clear that in time, the H-C foils become less DM and more FM.

4. Discussion and Conclusions

What is the nature of HTSC in these H-C materials? Following K. Onnes' discovery of SC in mercury below $T_c \simeq 4.19$ K (19), experimentalists and theorists as well have been strongly motivated to find and then explain the mechanism for new SC materials with higher T_c. In 1957, Bardeen, Cooper, and Schrieffer came up with the breakthrough BCS theory, in which the attractive interactions between electrons are explained as due to their interactions with the lattice excitations, i.e., with phonons (20). Following the

8

discovery of HTSC materials, it became clear that a new mechanism was needed, in which rather $e - e$ correlations than e-phonon interactions can lead to high T_c. In (1), we have discussed the case of HTSC in hydrogenated graphitic fibers on the basis of Little model for HTSC in organic materials (21). The model considers a molecular arrangement consisting of two parts: a) a long chain called the "spine" in which electrons fill the various states and may or may not form a conducting system; b) a series of arms or side chains attached to the spine. Under appropriate choice for the molecules which constitute the side chains, the virtual oscillation of charge in these side chains results in $e - e$ correlations, some of which are SC. Interestingly, even if the spine by itself is initially an insulator, the addition of side chains can increase the $e - e$ interactions to the point where it becomes energetically favorable to enter the SC state by mixing in states of the conduction band. The spine thus transforms from the insulating or semiconducting state directly to the SC metallic state upon the addition of the side chains. In the case of hydrogenated graphitic fibers or the graphite foil here, the treatment with octane results in the free protonation of octane at graphite's interfaces (22). The resulted superacidic protons (H+) move freely without activation energy on the graphite surface giving rise to HTSC. Thus, when Little s model is applied to the H-C foil, one can imagine that the spines are in the C planes with the protons as the arms or side chains. The free protons are shared by all C atoms in the plane to which the arms are connected to, thus the protons mediate $e - e$ correlations that need no input energy, i.e., they make the H-C foil SC. A similar phenomenon was found in (23). Thus, due to the off-diagonal long-range order that distinguished the SC from normal or insulating states, it is possible that Wigner s search for a quantum system to reproduce itself would lead to a SC as the only system where the probability for such an event would be nonzero. Wigner crystallization, which can be established in a pressurized twisted bilayer graphene, can lead to SC correlations (24). Usually, the formation of a Wigner crystal occurs when the system is under a magnetic field (25). As we have found, the magnetic field plays an important role in establishing SC correlations in hydrogenated graphites and other C-based materials (1; 5; 6; 7).

The results presented here on hydrogenated graphite foil are in agreement with our previous findings, thus confirming high-temperature superconductivity in hydrogenated graphitic materials with critical temperature $T_c \sim 50 - 60$ K. While upping the strength of the magnetic field, the temperature-dependent magnetization reveals several important transitions:

from a Néel paramagnetic-antiferromagnetic transition, to a ferromagnetic superconductor state, to an orbital paramagnetic glass high-temperature superconductor. The magnetization loops show the kink feature that is characteristic to granular superconductors and ferromagnetism extending up to room temperature. Indeed, when electron-electron correlations and magnetism walk in, these H-C organic materials might just "forge revolutionary paths in the quest for high-temperature superconductivity" (26).

[1] N. Gheorghiu, C.R. Ebbing, and T.J. Haugan, *Superconductivity in Hydrogenated Graphites*, **arXiv:2005.05876** (2020).

[2] A.C. Basaran, J.E. Villegas, J.S. Jiang, A. Hoffmann, and I.K. Schuller, *Mesoscopic magnetism and superconductivity*, MRS Bulletin, **40**, 92 (2015).

[3] N. Gheorghiu, C.R. Ebbing, and T.J. Haugan, *Electric-field induced strange metal states and possible high-temperature superconductivity in hydrogenated graphitic fibers*, **arXiv:2005.07885**, 2020.

[4] O.V. Yazyev, *Emergence of magnetism in graphene materials and nanostructures*, Rep. Prog. Phys. **73** 056501 (2010).

[5] N. Gheorghiu N, C.R. Ebbing, B.T. Pierce, and T.J. Haugan, *Quantum effects in graphitic materials: Colossal magnetoresistance, Andreev reflections, ferromagnetism, and granular superconductivity*, IOP Conf. Ser.: Mater. Sci. Eng. **756** 012022 (2020).

[6] N. Gheorghiu, C.R. Ebbing, J.P. Murphy, B.T. Pierce, T.J. Haugan, *Superconducting-like and magnetic transitions in oxygen-implanted diamond-like and amorphous carbon films, and in highly oriented pyrolytic graphite*, **arxiv: 2108.07417**, accepted for publication in Conf. Ser.: Mater. Sci. Eng. (2021-2022).

[7] N. Gheorghiu, C.R. Ebbing, and T.J. Haugan TJ, *Boron Content and the Superconducting Critical Temperature of Carbon-Based Materials*, **arXiv:2012.06624** (2020).

[8] Y. Kubozono et al., *Superconductivity in aromatic hydrocarbons*, Physica C **514**, 199 (2015).

[9] A. Tagliacozzo, G. Campagnano, D. Giuliano, P. Lucignano, and B. Jouault, *Thermal transport driven by charge imbalance in graphene in a magnetic field close to the charge neutrality point at low temperature: Nonlocal resistance*, Phys. Rev. B **99**, 155417 (2019).

[10] G. Baskaran, *Resonating-valence-bond contribution to superconductivity in MgB_2*, Phys. Rev. B **65**, 212505 (2002).

[11] Y. Yeshurun, I. Felner, and H. Sompolinsky, *Magnetic properties of a high-T_c superconductor $YBa_2Cu_3O_7$: Reentrylike features, paramagnetism, and glassy behavior*, Phys. Rev. B **36(1)**, 840 (1987).

[12] E.R. Podolyak, *On Magnetic Flux Trapping by Surface Superconductivity*, JEPT **126(3)**, 389 (2018).

[13] A.K. Geim, S.V. Dubonos, J.G.S. Lok, M. Henini, & J. C. Maan, *Paramagnetic Meissner effect in small superconductors*, Nature **396**, 144 (1998).

[14] B. Nagy et al., *On the explanation of the paramagnetic Meissner effect in superconductor/ferromagnet heterostructures*, EPL **116**, 17005 (2016).

[15] F. V. Kusmartsev, *Orbital Glass in HTSC: a New State of Condensed Matter*, J Supercond Nov Magn **5(5)**, 463 (1992).

[16] N. Garcia and P. Esquinazi, *Mean-Field Superconductivity Approach in Two Dimensions*, J Supercond Nov Magn **22**, 439 (2009).

[17] S. Kumar, R.P. Singh, A. Thamizhavel, C.V. Tomy, *Evidence of surface superconductivity and multi-quanta vortex states in a weakly-pinned single crystal of $Ca_3Ir_4Sn_{13}$*, Physica C **509**, 42 (2015).

[18] D. Saint-James and P.G. deGennes, *Onset of superconductivity in decreasing fields*, Phys. Lett. **7(5)**, 30 (1963).

[19] H.K. Onnes, Commun. Phys. Lab. Univ. Leiden. **120b**, **122c**, **122d** (1911).

[20] J. Bardeen, L. N. Cooper, and J. R. Schrieffer, *Theory of Superconductivity*, Phys. Rev. **108**, 1175 (1957).

[21] W.A. Little, *Possibility of Synthesizing an Organic Superconductor*, Phys. Rev. A **134(6A)**, 1416 (1964).

[22] Y. Kawashima & M. Iwamoto, *Protolytic decomposition of n-octane on graphite at near room temperature*, Sci. Rep. **6**, 28493 (2016).

[23] Y. Kawashima, *Superconductivity above 500 K in conductors made by bringing n-alkane into contact with graphite*, **arXiv:1612.05294** (2016).

[24] B. Padhi and P.W. Phillips, *Pressure-induced metal-insulator transition in twisted bilayer graphene*, Phys. Rev. B **99**, 205141 (2019).

[25] Yu P. Monarkha and V.E. Syvokon, *A two-dimensional Wigner crystal (review article)*, Low Temp. Phys. **38**, 1067 (2012).

[26] D. Jérome, *Organic Superconductors: When Correlations and Magnetism Walk in*, J Supercond Nov Magn **25**, 633 (2012).
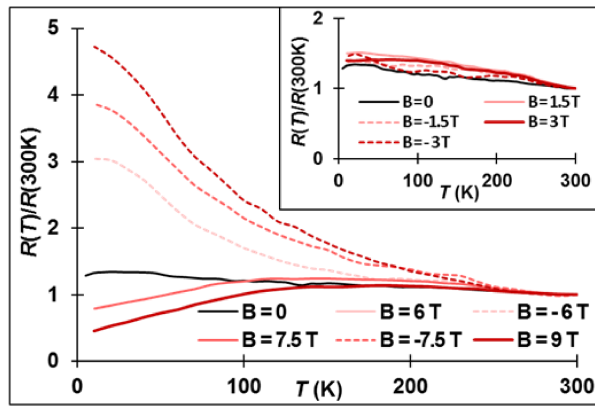
Figure 1: Temperature-dependent resistance (normalized to the value at 300 K) for a raw H-C foil in perpendicular magnetic field. The inset shows that lower B has a less significant effect R.
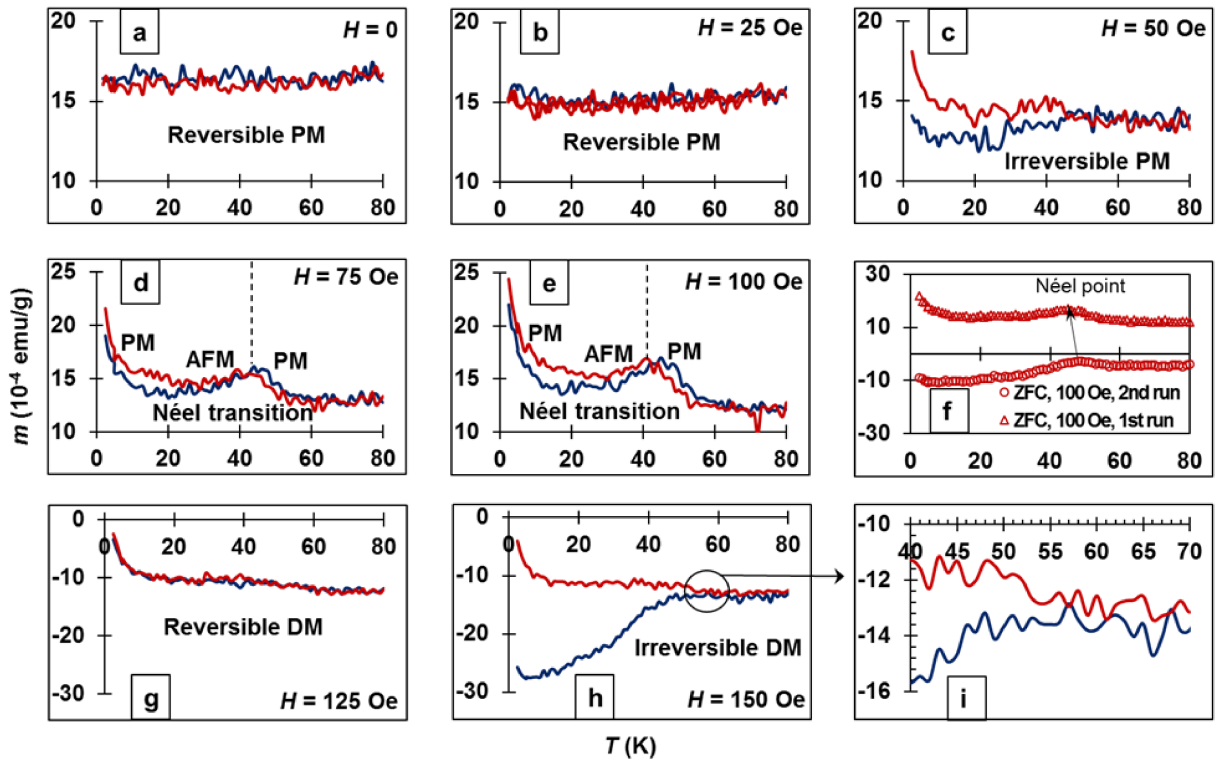
Figure 2: ZFC-FC low-field data for the H-C foil. As the strength of the magnetic field H is increased, several magnetic transitions are observed: reversible to irreversible paramagnetic (PM) (a-c), to slightly irreversible PM-AFM Néel transition (d-f), to reversible DM (2g), and finally to irreversible DM (h-i).

14
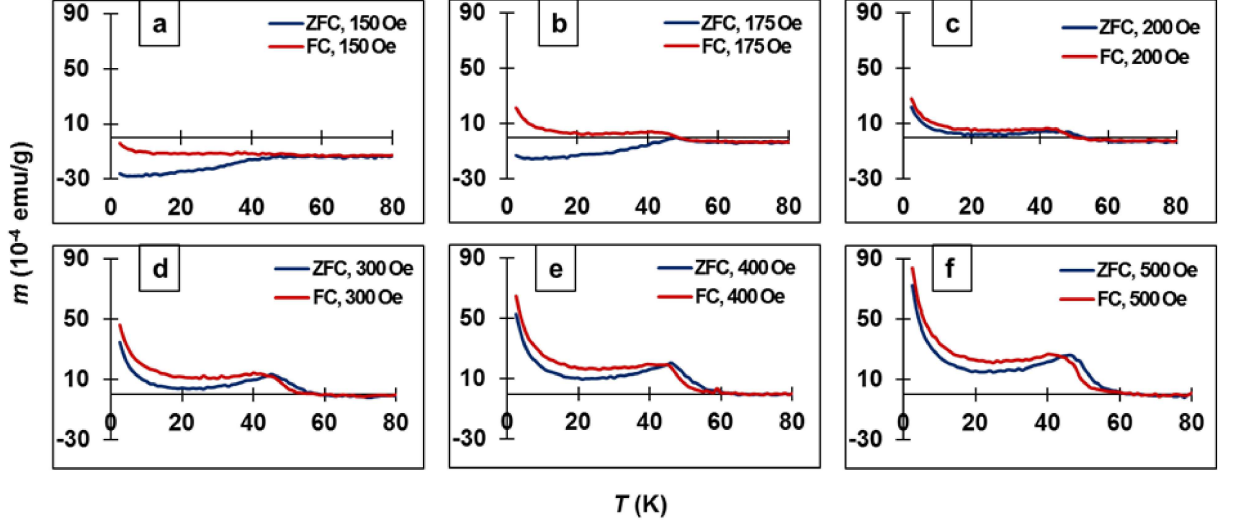
Figure 3: ZFC-FC high-field data for the H-C foil. For comparison with Fig. 2, the $H = 150$ Oe data was again included. With the strength of the magnetic field H further increased, several magnetic transitions are observed: irreversible DM (3a), to irreversible PM-DM (3b), to practically reversible PM (3c), to slightly irreversible PM-AFM Néel transition (3d-f).
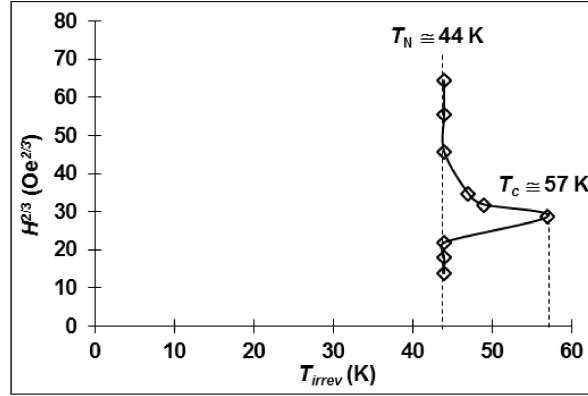
Figure 4: The H-C foil is not a glass system, as $H^{2/3}(T)$ is not an Almeida-Thouless line. The reentrance of PM followed by more PM-AFM Néel transitions suggests that the H-C foil might be an orbital glass HTSC, where orbital PM order and SC order coexist without the Meissner effect.

15
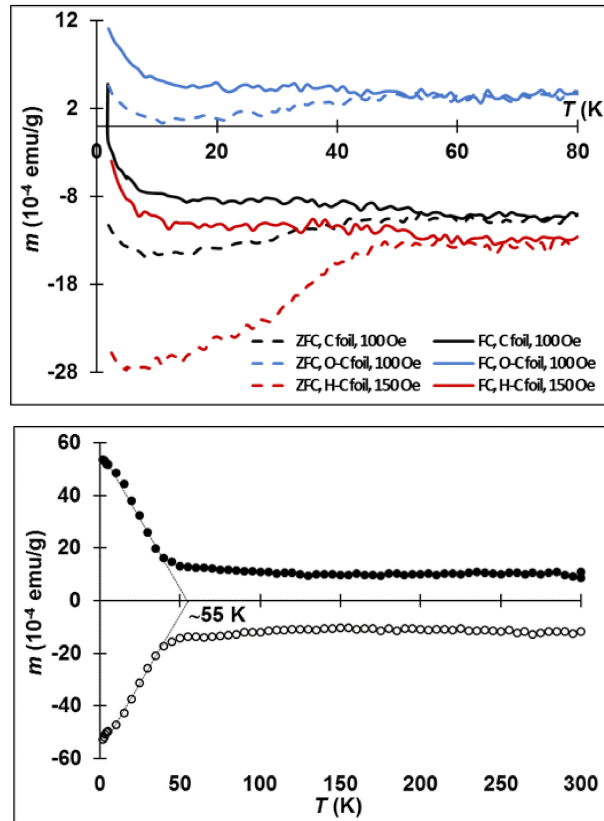
Figure 5: Upper plot: ZFC-FC data for a raw C foil (in black), O-implanted C foil (O-C foil, in blue)), and hydrogenated C foil (H-C foil, in red), respectively. Lower plot: Remanent magnetization for a raw C foil sample obtained after the application of a field of induction $B_+ = 9$ T (filled symbols) and $B_- = -9$ T (empty symbols), respectively.
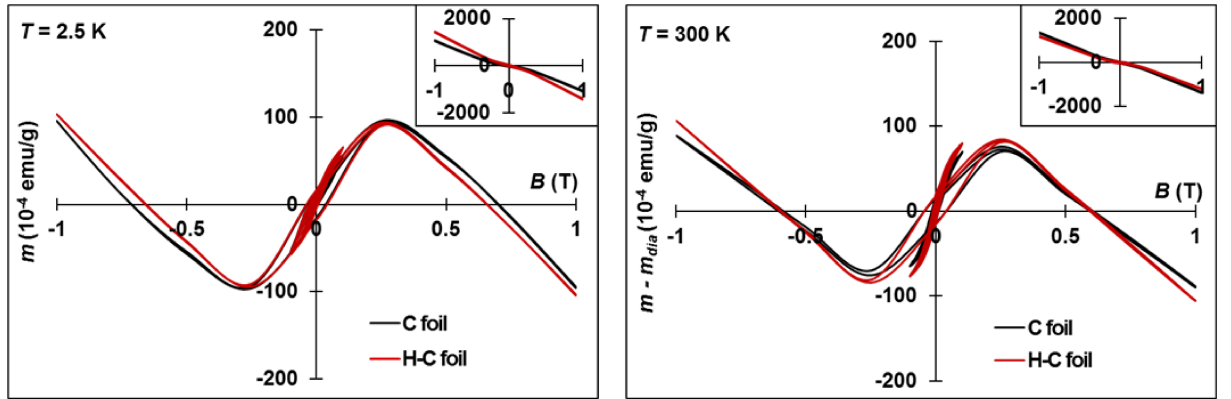
16

Figure 6: High-field magnetization loops $m(B)$ for $T = 2.5$ K and $T = 300$ K, respectively. Legend: raw C foil in black and H-C foil in red. DM background included (left) vs. DM background (inset) subtracted (right).
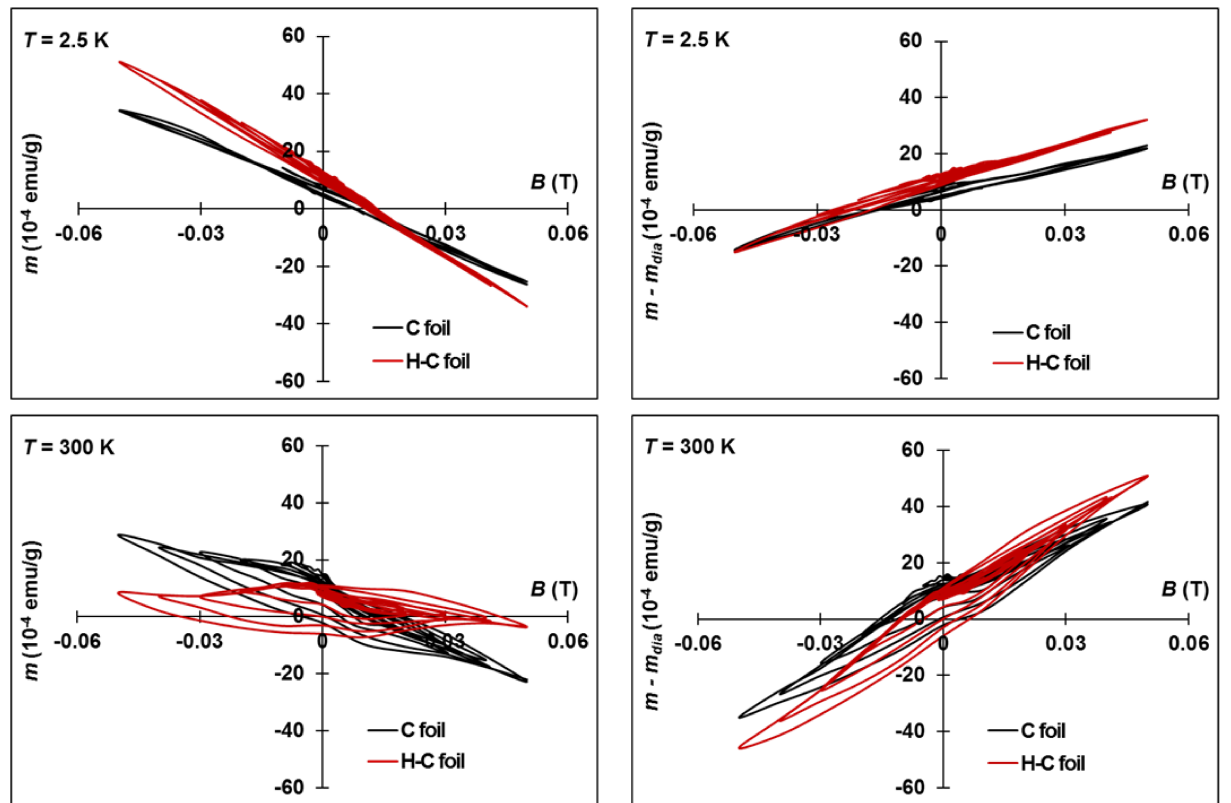
Figure 7: Low-field magnetization loops $m(B)$ for $T = 2.5$ K and $T = 300$ K, respectively. DM background included (left) vs. DM background (inset) subtracted (right).
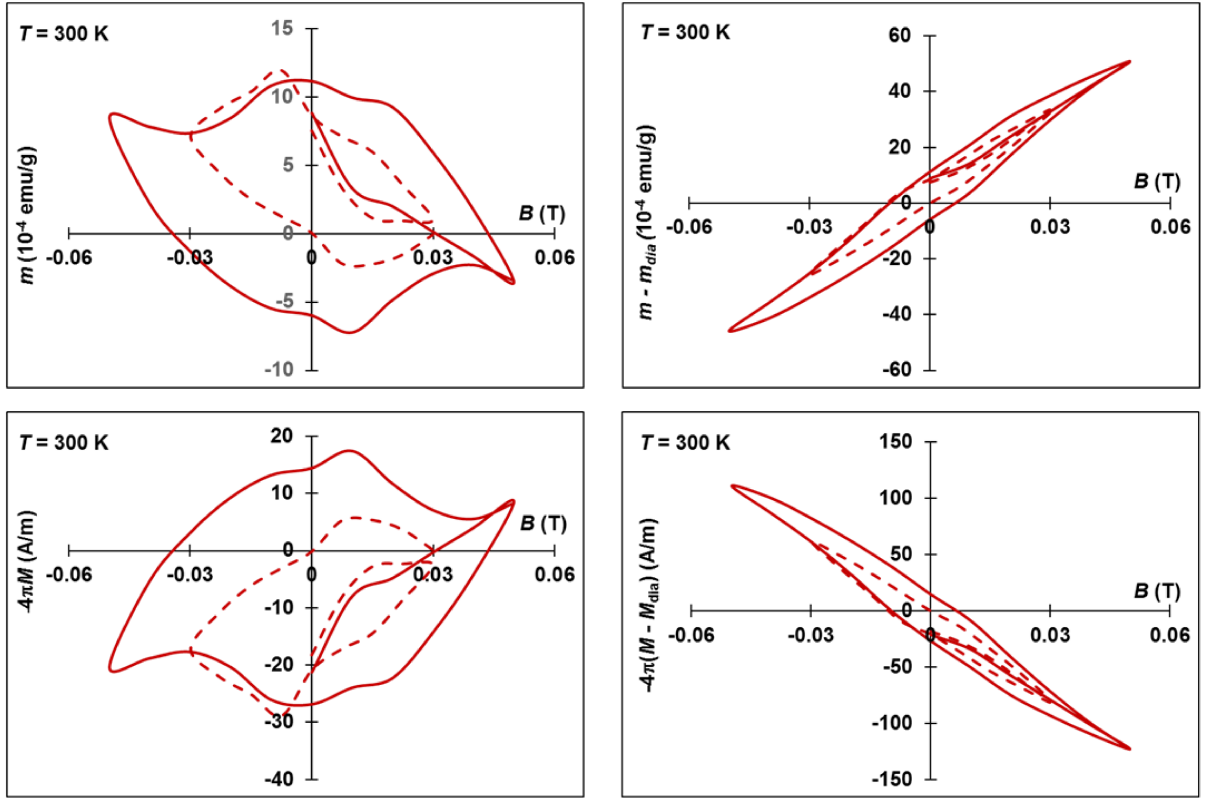
17

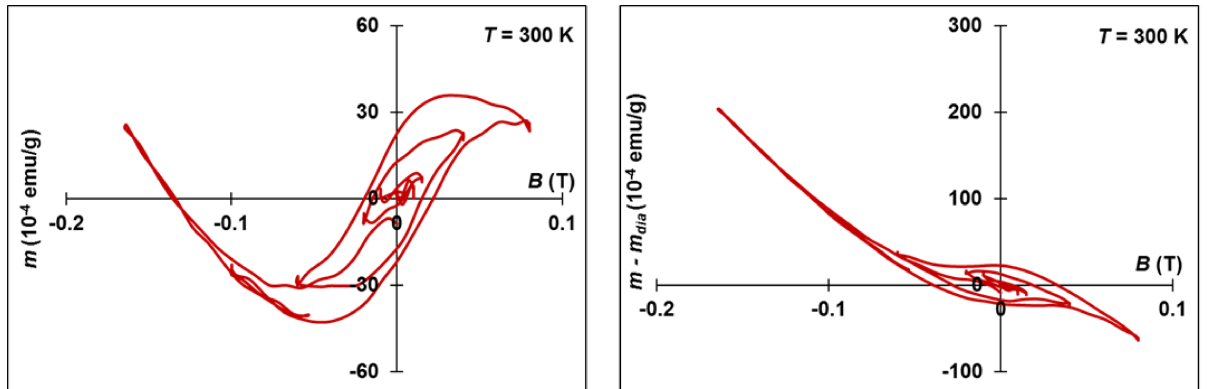Figure 8: Magnetization loops (upper plots) and magnetic moment (bottom plots) at $T = 300$ K.

Figure 9: Degaussing of the H-C foil. The magnetic field H was ramped down to zero in an oscillatory manner at a rate -100 Oe/s, from 0 to -1000 Oe, to 800 Oe, to -600 Oe, to 400 Oe, to -200 Oe, to 0. The trend is as expected because m is linear in H (or B). The data is shown both with (left) and without (right) DM background, respectively.
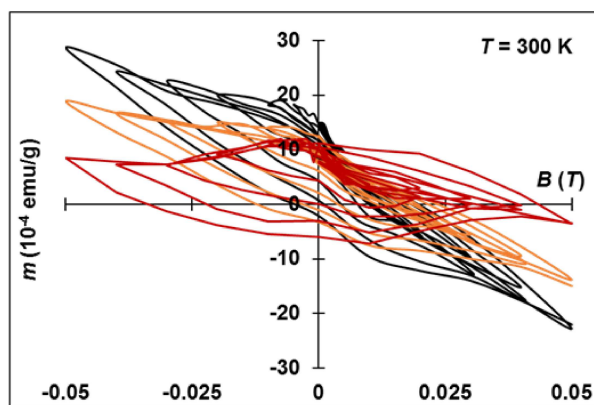
18

Figure 10: The effect of octane-intercalation period on the H-C foil. Legend: seven months (red) vs. thirteen months (orange) vs. no intercalation (black).